

100 Gbit/s Electro-Optic Modulator and 56 Gbit/s All-Optical Wavelength Converter In Silicon-Organic Hybrid (SOH) Technology

W. Freude, J. Leuthold, L. Alloatti, T. Vallaitis,
D. Korn, R. Palmer, C. Koos
Karlsruhe Institute of Technology (KIT)
Institute of Photonics and Quantum Electronics (IPQ)
D-76131 Karlsruhe, Germany
www.ipq.kit.edu — w.freude@kit.edu

P. Dumon, R. Baets
Photonics Research Group, Ghent University — IMEC
Dept. of Information Technology
B-9000 Gent, Belgium

B. Breiten, F. Diederich
ETH Zürich
Laboratorium für Organische Chemie
CH-8093 Zürich, Switzerland

J.-M. Brosi

Karlsruhe Institute of Technology (KIT)
Institute of Photonics and Quantum Electronics (IPQ)
Now with: Robert Bosch GmbH, Power Tools Division
D-70771 Leinfelden-Echterdingen, Germany

M. L. Scimeca, I. Biaggio
Department of Physics
Lehigh University
Bethlehem, PA 18015, USA

A. Barklund, R. Dinu, J. Wieland
GigOptix Inc., Bothell (WA), USA
GigOptix-Helix AG
CH-8008 Zürich, Switzerland

Abstract—CMOS-compatible silicon photonics combined with covers of $\chi^{(2)}$ or $\chi^{(3)}$ -nonlinear organic material allows electro-optic modulators and all-optical wavelength converters for data rates of 100 Gbit/s and beyond. The devices are not impaired by free carriers.

Keywords-silicon photonics; modulator; four-wave mixing

I. INTRODUCTION

Silicon-on-insulator (SOI) photonics represents a CMOS-compatible and therefore cost-effective technology for fabricating devices like modulators and all-optical wavelength converters (AOWC) in the wavelength region near $\lambda = 1.55 \mu\text{m}$. The large refractive index ($n_{\text{Si}} = 3.5$) of silicon provides the strong light confinement and the high intensities that are desirable for nonlinear interactions. However, the $\chi^{(2)}$ -susceptibility of silicon, which would be required for electro-optic modulators, is negligibly small. As a consequence, plasma-effect based modulators [1] [2] were developed, but they suffer from speed limitations associated with charge carrier injection and removal. A similar speed problem arises when exploiting the large $\chi^{(3)}$ -nonlinearity of silicon [3], because two-photon absorption (TPA) generates free carriers with long life times leading to absorption (FCA) as well as bit pattern dependent phase shifts. So intensities have to be kept low, or the carriers must be removed by pn-junctions [4]. Our approach employs silicon-organic hybrid (SOH) systems and combines silicon waveguides with a highly $\chi^{(2)}$ -nonlinear electro-optic organic material [5–9], or with a Kerr-type $\chi^{(3)}$ -nonlinear [9–14] organic cover, which reacts virtually instantaneously, has a low refractive index and does not suffer from TPA.

II. ELECTRO-OPTIC MODULATOR

Fig. 1(left) shows the SOH slot structure of a phase modulator (PM). The light is guided (effective refractive index $n_{\text{opt,eff}} = 2.9$) by silicon strips which are embedded in an electro-optic material (EO). Field discontinuities at the high index-contrast Si-EO interfaces lead to a strong field enhancement

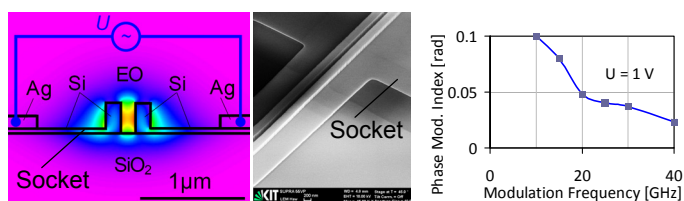


Figure 1. Phase modulator (PM) schematic with $\chi^{(2)}$ -nonlinear SOH slot waveguide (left) PM with doped-socket waveguide, colour-coded quasi-TE field magnitude, electro-optic organic material EO (centre) SEM image of PM without metallization (right) Optical phase modulation index η vs. modulation frequency f for various on-chip RF voltage amplitudes. Rapid decrease of η with f by strong reflections at open end of broken RF electrodes.

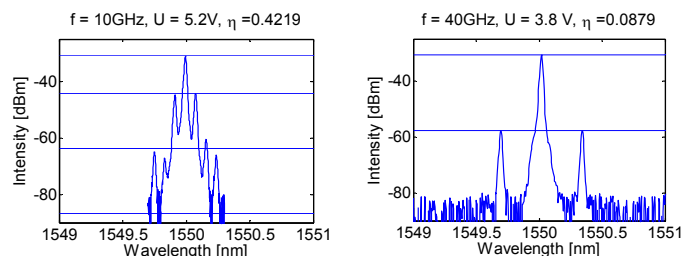


Figure 2. Optical spectra for phase modulation at frequency f (left) $f = 10 \text{ GHz}$, RF amplitude $U = 5.2 \text{ V}$ (right) $f = 40 \text{ GHz}$, $U = 3.8 \text{ V}$

between the strips. The modulating RF field (effective refractive index $n_{\text{el,eff}} = 2.5$) is applied via two silver electrodes, which are connected to the $L = 4$ mm long strips by two 70 nm high and 2 μm wide sockets. The whole structure is As-doped to make it conductive without introducing too much optical loss. An SEM picture of the PM without metallization is displayed in Fig. 1(centre). During the metallization process, the electrodes broke at the far end of the slot region so that no impedance matching resistance could be connected. As a consequence, the modulator does not operate in a travelling-wave mode as intended, but suffers from strong reflections at the open end of the transmission line. We measured the phase modulation index η by applying a sinusoidal RF voltage with amplitude U and frequency f . For small f the open-circuit reflection doubles the nominal modulation voltage U while this effect disappears asymptotically for large f , Fig. 1(right). Electrode losses start increasing for $f > 30$ GHz.

Measured optical spectra at $f = 10$ GHz; 40 GHz are shown in Figure 2. The phase modulation index η was determined by evaluating the ratio of the heights of the central peak $J_0^2(\eta)$ and of the first sidebands $J_1^2(\eta)$ in Figure 2. ($J_\nu(\eta)$ are Bessel functions of order ν). The quantity U_π is the voltage resulting in a phase change of $\eta = \pi$. The smallest U_π voltage we observed so far is $U_\pi / L = 5 \text{ V} / 4 \text{ mm}$. However, there are many opportunities for optimization. The value U_π is essentially determined by the effective electro-optic coefficient $r_{33} = 150 \text{ pm/V}$ which in turn is adjusted to its full value by appropriately poling [7] the EO material, e. g. with a DC voltage at elevated temperature.

An amplitude modulator can be formed by inserting a PM in both arms of an Mach-Zehnder interferometer as in the schematic Fig. 3(left). The bandwidth $f_{3\text{dB}}$ due to walk-off between the optical field and the RF forward-travelling wave (negative sign) or a potentially reflected wave (positive sign) is well approximated by [6] (vacuum speed of light c)

$$f_{3\text{dB}} \approx 0.5 \frac{c}{L} \frac{1}{|n_{\text{opt,eff}} \mp n_{\text{el,eff}}|}.$$

With the data above and in a true travelling-wave configuration, a limiting modulation frequency of $f_{3\text{dB}} \approx 94$ GHz is to be expected. The RC roll-off frequency is even larger (about 150 GHz). This modulation bandwidth would be more than sufficient for a data rate of 100 Gbit/s. A 40 Gbit/s modulator was already reported [8].

In the specific case of Fig. 3 the PM is a slotted slow-light photonic crystal. We expect [6] a modulation rate of 100 Gbit/s at a voltage amplitude of 1 V and an optical bandwidth 2 THz.

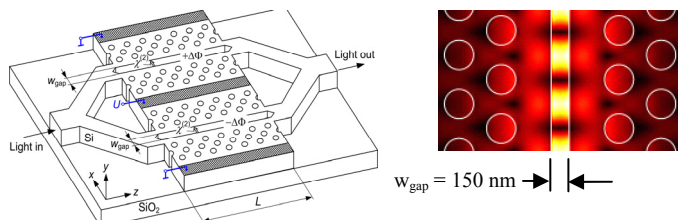


Figure 4. Mach-Zehnder modulator schematic (left) Modulator with slotted photonic-crystal phase modulator sections (length $L = 80 \mu\text{m}$) covered by a $\chi^{(2)}$ -nonlinear organic material (right) Colour-coded electric field magnitude of quasi-TE mode in phase modulator section

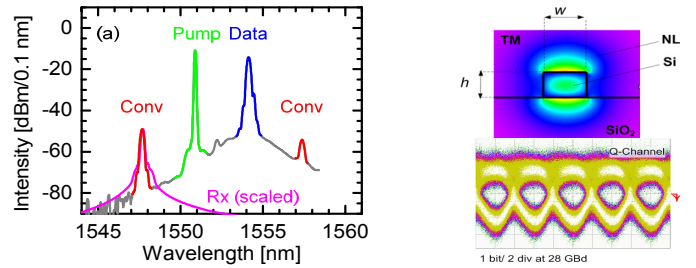


Figure 3. FWM wavelength conversion of 56 Gbit/s NRZ-DQPSK data (left) Spectra after waveguide and in receiver (Rx) (upper right) SOH strip waveguide with quasi-TM electric field magnitude. Nonlinear organic cover (NL), $h = 220 \text{ nm}$, $w = 400 \text{ nm}$, $L = 4 \text{ mm}$ (lower right) eye diagram of quadrature signal at 1547.7 nm, BER = 10^{-5} , quality is Rx-noise limited.

III. FWM WAVELENGTH CONVERSION OF DQPSK DATA

For wavelength conversion of phase-encoded DQPSK signals the phase information must be conserved. This can be achieved by four-wave mixing (FWM) in an SOH strip waveguide that is simple to fabricate. The silicon strip is covered with a highly nonlinear organic material (DDMEBT) [10], Figure 3. The device is operated in quasi-TM mode to reduce linear losses (1 dB/mm). The TPA figure of merit $\text{FOM}_{\text{TPA}} = 1.2$ [13] is sufficient for all-optical signal processing. NRZ-DQPSK data (56 Gbit/s, +16 dBm) and CW pump (+19 dBm) enter the strip and lead to a converted signal [14], Fig. 4(left). The quadrature channel data are displayed in Fig. 4 (lower right). No bit pattern distortions are observed. Improving the 20 dB fiber-to-fiber loss would result in error-free transmission and in bitrates of 100 Gbit/s and beyond [12].

ACKNOWLEDGMENT

We acknowledge support by the DFG Center for Functional Nanostructures (CFN), the DFG Priority Program SP 1113 "Photonic Crystals", the KIT Initiative of Excellence, the EU-FP7 projects EUROFOS (grant 224402), SOFI (grant 248609), and by Deutsche Telekom Stiftung. We are grateful for technological support by the Light Technology Institute (KIT-LTI) and the ePIXfab (silicon photonics platform). I. B. and M. L. S. acknowledge support from the Commonwealth of Pennsylvania, Ben Franklin Technology Development Authority. F. D. acknowledges support from the ETH research council.

REFERENCES

- [1] L. Liao et al., Electron. Lett., vol. 43, no. 22, 20072253, 2007. Digital Object Identifier <http://dx.doi.org/10.1049/el:20072253>
- [2] W. M. J. Green et al., Opt. Express, vol. 15, no. 25, 17106-17113, 2007. doi:10.1364/OE.15.017106
- [3] R. Salem et al., Nature Photon., vol. 2, 35-38, 2008. doi:10.1038/nphoton.2007.249
- [4] H. Rong et al., Nature, vol. 433, 292-294, 2005. doi:10.1038/nature03273
- [5] C. Koos et al., ECOC 2007, paper P056.
- [6] J.-M. Brosi et al., Opt. Express, vol. 16, no. 6, 4177-4191, 2008. doi:10.1364/OE.16.004177
- [7] E. M. McKenna et al., J. Opt. Soc. Am. B, vol. 24, no. 11, 2888-2892, 2007. doi:10.1364/JOSAB.24.002888
- [8] H. Chen et al., Appl. Phys. Lett., vol. 93, 043507, 2008. doi:10.1063/1.2965809
- [9] J. Leuthold et al., Proc. IEEE, vol. 97, no. 7, 1304-1316, 2009. doi:10.1109/JPROC.2009.2016849
- [10] B. Esembeson et al., Adv. Mater., vol. 20, no. 23, 4584-4587, 2008. doi:10.1002/adma.200801552
- [11] C. Koos et al., Opt. Express, vol. 15, no. 10, 5976-5990, 2007. doi:10.1364/OE.15.005976
- [12] C. Koos et al., Nature Photon., vol. 3, 216-219, 2009. doi:10.1038/nphoton.2009.25
- [13] T. Vallaitis et al., Opt. Express vol. 17, 17357-17368, 2009. doi:10.1364/OE.17.017357
- [14] T. Vallaitis et al., OFC 2010, Paper OTuN1 [www.opticsinfobase.org/browseconferences.cfm?meetingid=5&strYr=2010](http://www.opticsinfobase.org/browseconferences/cfm?meetingid=5&strYr=2010)